Optical properties of a square-lattice photonic crystal within the partial bandgap

Zhixiang Tang, Runwu Peng, Yunxia Ye, Chujun Zhao, and Dianyuan Fan

Shanghai Institute of Optics and Fine Mechanics, Chinese Academy of Sciences, P.O. Box 800-211, Shanghai 201800, China

Hao Zhang

Department of Optical Science and Engineering, Fudan University, Shanghai 200433, China

Shuangchun Wen

School of Computer and Communication, Hunan University, Changsha 410082, China

Received March 22, 2006; revised August 12, 2006; accepted August 13, 2006; posted August 21, 2006 (Doc. ID 69171); published January 10, 2007

Optical properties of a two-dimensional square-lattice photonic crystal are systematically investigated within the partial bandgap through anisotropic characteristics analysis and numerical simulation of field pattern. Using the plane-wave expansion method and Hellmann–Feynman theorem, the relationships between the incident and refracted angles for both phase and group velocities are calculated to analyze light propagation from air to photonic crystals. Three kinds of flat slab focusing are summarized and demonstrated by numerical simulations using the multiple scattering method. © 2007 Optical Society of America

OCIS codes: 290.4210, 110.2960, 260.2110.

1. INTRODUCTION

A photonic crystal (PhC) is an artificial medium whose refractive index is periodically arranged.[1,2] When propagating through this medium, electromagnetic waves will be modulated in the form of Bloch modes and photonic band structure appears. Due to the multiple scattering in PhC, anomalous electromagnetic phenomena such as the so-called negative refraction and its resulted flat slab focusing can be present.[3,4] Negative refraction is one of the unusual characteristics of left-handed materials, which were initially proposed by Veselago in the 1960s (Ref. 5) and have attracted renewed interest recently.[6–12] In general, an isotropic left-handed medium results in negative refraction. However, there is no necessary relation between the refraction and rightness for anisotropic mediums.[13] Take the anisotropic PhC as an example. Because of the Bloch phase and group velocities being noncollinear, both left-handed positive refraction and right-handed negative refraction can occur.

Usually, there are two kinds of negative refraction and its resulting focusing effect in PhCs.[4,10,14] One is the left-handed behavior as described by Veselago. In this case, the electromagnetic fields $\mathbf{E}$ and $\mathbf{H}$ and the wave vector $\mathbf{k}$ form a left-handed triplet (i.e., $\mathbf{S}\cdot\mathbf{k}<0$, where $\mathbf{S}$ is the Poynting vector). This kind of negative refraction in PhCs was first pointed out by Notomi,[3] and has been demonstrated by lots of numerical simulations and experiments.[11–15] The other is realized without employing negative index or left-handed behavior, but by the high-order Bragg scattering[10] or anisotropy.[4] In the latter case, the PhC behaves much like a right-handed medium (i.e., $\mathbf{S}\cdot\mathbf{k}>0$). This kind of negative refraction and its resulting focusing were first theoretically investigated in the partial bandgap of a two-dimensional (2D) square-lattice PhC in 2002, and was experimentally confirmed one year later.[8,9] Subsequently, much attention has been focused on such PhC arrays.[16–19] Recently Li *et al.* have studied these extraordinary phenomena in PhCs made by cylindrical rods in a triangular lattice and elliptical rods in a square lattice[20,21] that differ from squares-lattice PhCs with cylindrical rods studied intensively before and again in this paper.

Instead of analyzing the photonic band structure and equifrequency contours (EFCs) qualitatively as before, in this paper we investigate optical properties of a square-lattice PhC in the partial bandgap by using the plane wave expansion method and Hellmann–Feynman theorem to analyze the Bloch group velocities.[22] Based on the calculated results of the incident and refracted angles of group velocities, three kinds of flat slab focusing are summarized and demonstrated by numerical simulations using the multiple scattering methods.[19,23] Particularly, a right-handed flat lens that behaves like a left-handed optically thinner medium is discussed.

2. ANISOTROPIC CHARACTERISTICS ANALYSIS

The 2D PhC considered in this paper consists of square-lattice dielectric cylinders arranged in the background of air. The cylinder has a dielectric constant of $\varepsilon=12.96$ and a radius of $r=0.3a$, where a is the lattice constant. Using

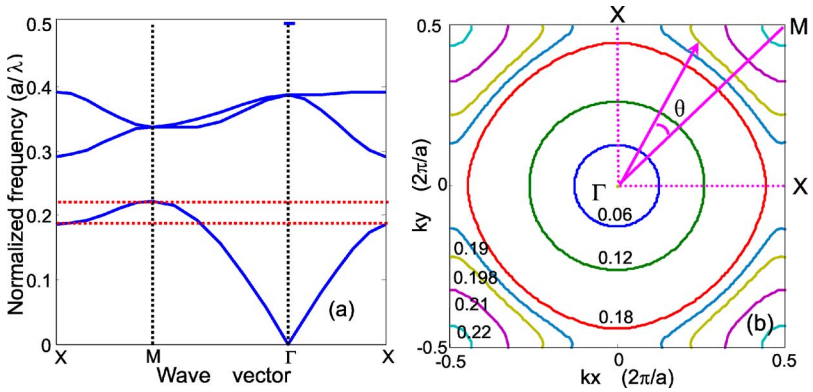

Fig. 1. (Color online) (a) Photonic band structure and (b) EFCs for the 2D PhC studied in this paper.

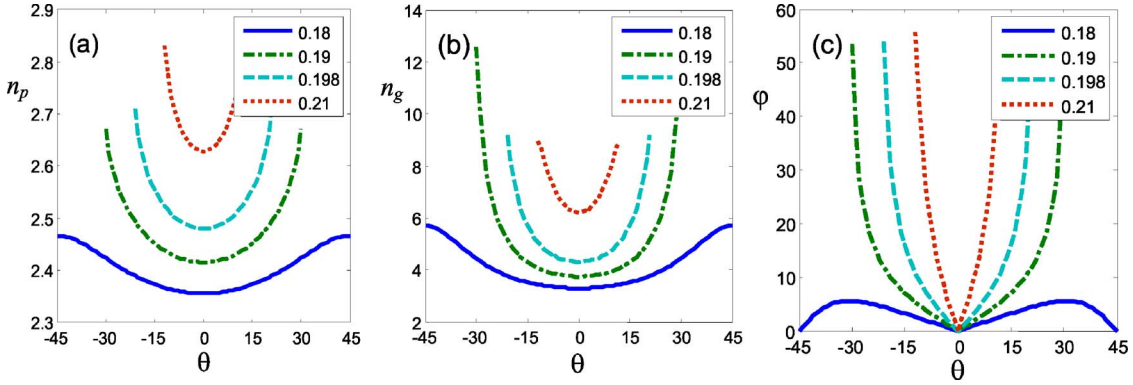

Fig. 2. (Color online) Schematics of anisotropy analyses for four Bloch modes such as f=0.18, 0.19, 0.198, and 0.21 (a) Phase indices n_p. (b) Group indices n_g. (c) Angles between the Bloch wave vector $\mathbf{k}$ and its corresponding group velocity v_g.

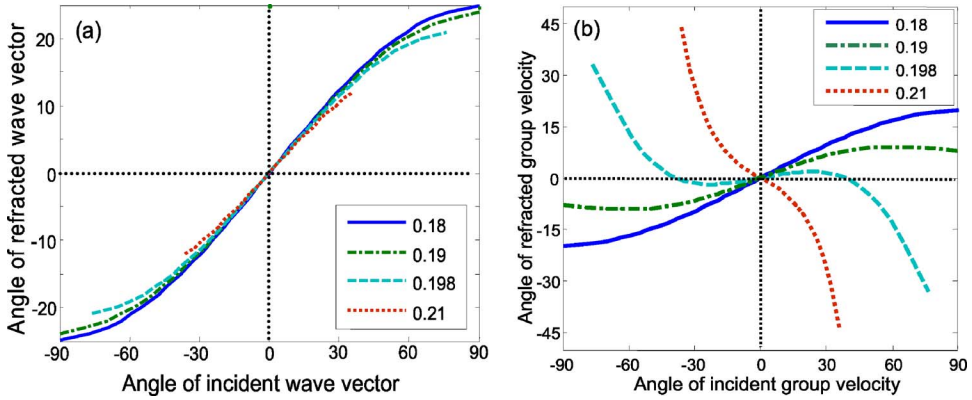

Fig. 3. (Color online) Schematics of the incident angle in free space and its corresponding refracted angle in PhC for (a) phase velocities and (b) group velocities.

the plane-wave expansion method, photonic band structure and EFCs for the TM polarization are calculated and plotted in Fig. 1. The frequency is normalized as a/λ and the interface between PhC and free space is along the ΓM direction. According to Notomi's theory, we can conclude from Fig. 1(b) that in the first band the PhC behaves right-handed, i.e., $\mathbf{S}\cdot\mathbf{k}>0$. In the partial bandgap (normalized frequency from 0.185 to 0.222), EFCs within the first Brillouin zone (BZ) are significantly distorted from a circle, indicating strong anisotropy. In this case, the Bloch group velocities normalized to the EFCs are no longer collinear with their corresponding phase velocities, and negative refraction can occur under certain conditions.

Considering the symmetry of a square lattice, we calculate the phase and group indices within a quarter BZ to analyze the anisotropic characteristics (i.e., the angle θ between the Bloch wave vector and the interface normal increases from $-\pi/4$ to $\pi/4$). The phase index[24] can be written as

$$n_p = \frac{\mathbf{k}}{\mathbf{k}_0} = \mathrm{sgn}(\mathbf{k}\cdot v_g)\frac{|\mathbf{k}|}{|\mathbf{k}_0|}, \tag{1}$$

where $\mathbf{k}$ and $\mathbf{k}_0$ are the wave vectors of light in PhC and free space respectively, and sgn is the sign function. v_g is the group velocity in PhC, which is given by

$$v_g = \nabla_k \omega(k). \tag{2}$$

The group index[22] is defined from the group velocity

$$n_g = c/|v_g| = c/|\nabla_k \omega(k)|, \tag{3}$$

where c is the velocity of the light in free space. Using the plane wave expansion method and Hellman–Feynman theorem,[22] the calculated results of n_p and n_g are shown in Figs. 2(a) and 2(b). In order to directly exhibit the Bloch phase and group velocities being noncollinear, the angle φ between these two vectors is plotted in Fig. 2(c).

These parameters of four normalized frequencies such as $f=0.18$, 0.19, 0.198, and 0.21 are shown in Fig. 2. For $f=0.18$ in the first conducted band, whose EFC is nearly a circle as shown in Fig. 1(b), the phase and group indexes vary slightly and the Bloch wave vectors are almost collinear with their corresponding group velocities. At this long wavelength, the PhC can be treated approximately as a homogenous isotropic medium characterized by an effective index. However, because of strong anisotropy in the partial bandgap, these parameters change fast, especially at the edges of the BZ. In this instance, the effective medium theory becomes invalid. To get an intuitive knowledge of light propagation from air to PhC, the relationships between the incident and refracted angles for both phase and group velocities are calculated and shown in Fig. 3.

In Fig. 3(a), all incident phase velocities at these four frequencies are refracted almost at the same positive direction for the same incident angle because their phase indexes are almost equal as shown in Fig. 2(a). But it is totally different for the group velocities. From Fig. 3(b), we can conclude three kinds of group refractions. For $f=0.19$, due to the convex and flat EFC as illustrated in Fig. 1(b), all incident beams are refracted positively but confined near the interface normal (the group refracted angles are less than 10°). At this frequency, near-field focusing can be present only for some thin slabs. As has been studied intensively before, a typical canalization effect occurs at $f=0.198$. Most of the incident beams are bent in the direction of ΓM. For the Bloch wave at the edge of the BZ being excited, negative refraction can take place as has been demonstrated experimentally in Ref. 8. At $f=0.21$, in some respects the PhC behaves like a left-handed optically thinner medium though $\mathbf{S}\cdot\mathbf{k}>0$. Negative refraction occurs when a plane wave is incident from air to PhC with an angle less than the critical angle.

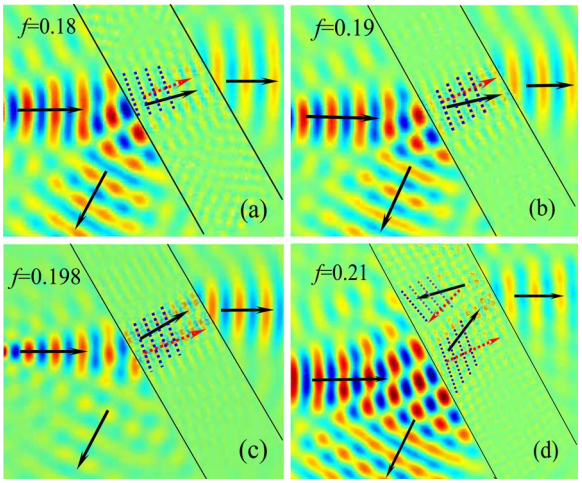

Fig. 4. (Color online) Refractions of a slit beam with an incident angle $\beta=30°$ at the normalized frequencies: (a) $f=0.18$, (b) $f=0.19$, (c) $f=0.198$, and (d) $f=0.21$. Blue dashed lines and red dashed and black arrows indicate the equiphase surfaces, phase velocities, and energy flows, respectively.

3. NUMERICAL SIMULATIONS

To test the above analysis, numerical simulations are conducted by using the multiple scattering method. First, we consider a slit beam[23] incident on a PhC slab with an angle $\beta=30°$ to the interface normal. Refractions for four normalized frequencies such as $f=0.18$, 0.19, 0.198, and 0.21 are illustrated in Fig. 4. Isophases, phase velocities, and energy flows are indicated by blue dashed lines and red dashed and black arrows, respectively. Although the theoretical results in Section 2 are calculated for infinite PhCs, they are still well consistent with these numerical simulations. Positive refractions at $f=0.18$, 0.19, canalization effect at $f=0.198$, and negative refraction at $f=0.21$ are demonstrated in Figs. 4(a)–4(d), respectively.

For investigating the imaging properties of a flat slab made from this PhC, a point source is located at $d_o=1.5a$ away from the center of the first row. For the point source with $f=0.18$, at which the PhC behaves like an almost isotropic right-handed medium, no focusing is

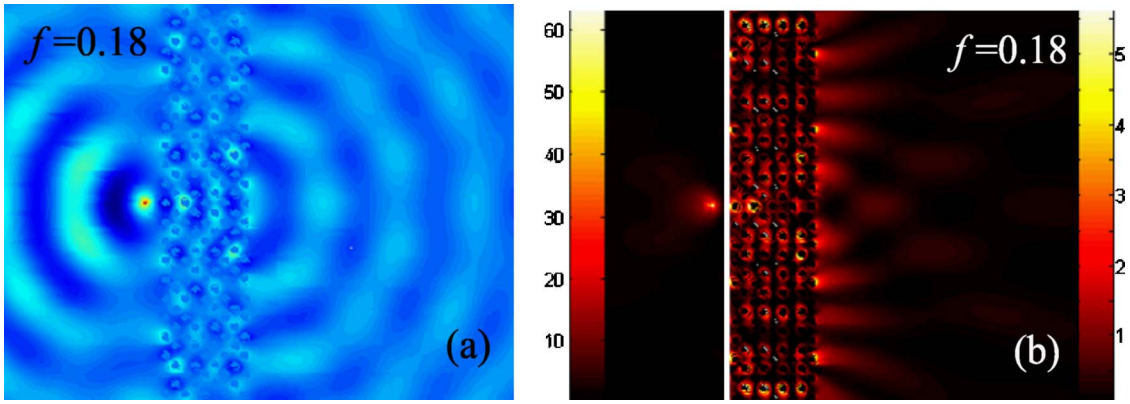

Fig. 5. (Color online) Distributions of (a) electric field amplitude and (b) intensity for a nine-layer PhC slab excited by a point source at $f=0.18$.

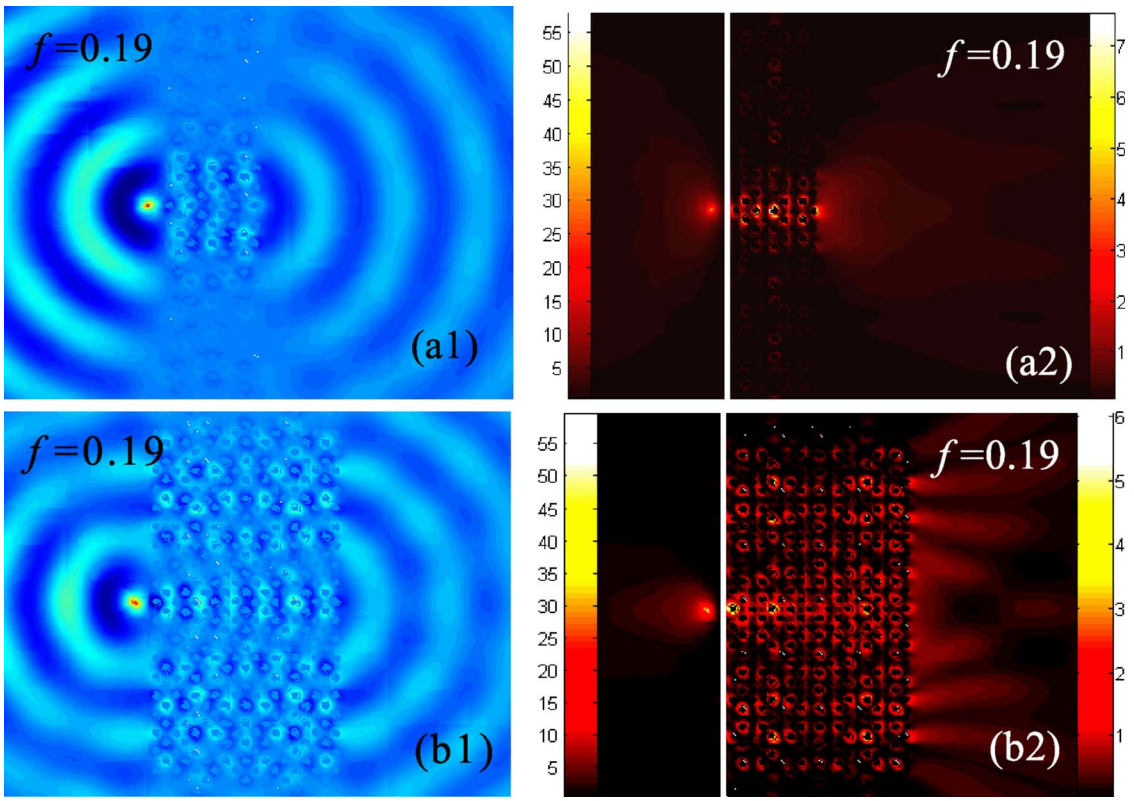

Fig. 6. (Color online) Propagation maps for (a) 9-layer and (b) 19-layer PhC slabs excited by a point source at $f=0.19$. (a1) and (b1) are the snapshots of the electric field amplitude. (a2) and (b2) display the corresponding intensity distributions.

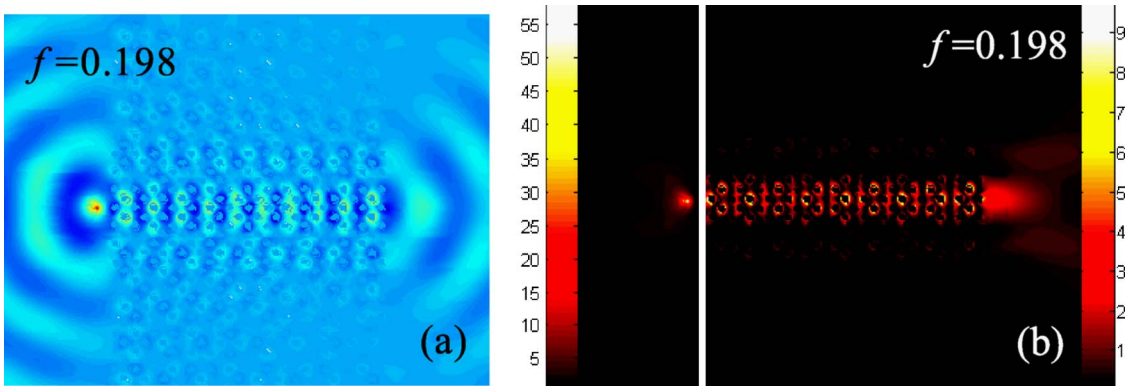

Fig. 7. (Color online) Distributions of (a) electric field amplitude and (b) intensity for a 29-layer PhC slab excited by a point source at $f=0.198$.

present as depicted in Fig. 5. In Fig. 6(a), an image is formed behind a nine-layer PhC slab due to the weak canalization effect at $f=0.19$. When the slab is added to 19 layers, the image disappears as shown in Fig. 6(b). At the typical canalization frequency $f=0.198$, an image appears even for a 29-layer slab as illustrated in Fig. 7. A guiding channel is clearly visible through the PhC slab.

For the PhC slab lens at $f=0.21$, the dependence of the image on the object distance and slab thickness is demonstrated in Fig. 8. This kind of imaging is obviously different from the near-field focusing caused by canalization effects. As shown in Fig. 8(a), a point source is located before a 17-layer PhC slab at $d_o=1.5a$, and an image is formed at $d_i=7.5a$ away from the center of the last row. Then, we relocate the point source at $d_o=6a$ to increase the object distance beyond the near-field region. It is clear in Fig. 8(b) that the image moves forward to $d_i=6.4a$. Finally, the slab lens is added to 29 layers, and the image is evidently backed off at $d_i=12.9a$ as depicted in Fig. 8(c). These phenomena are similar to the geometric optics analysis for a negative-index slab with $|n|<1$.

4. CONCLUSION

In conclusion, we have systematically investigated the optical properties of a 2D square-lattice PhC within the partial bandgap by analyzing the Bloch group velocities. The relationships between the incident and refracted angles for both phase and group velocities have been obtained to get an intuitive knowledge of light propagation from air to

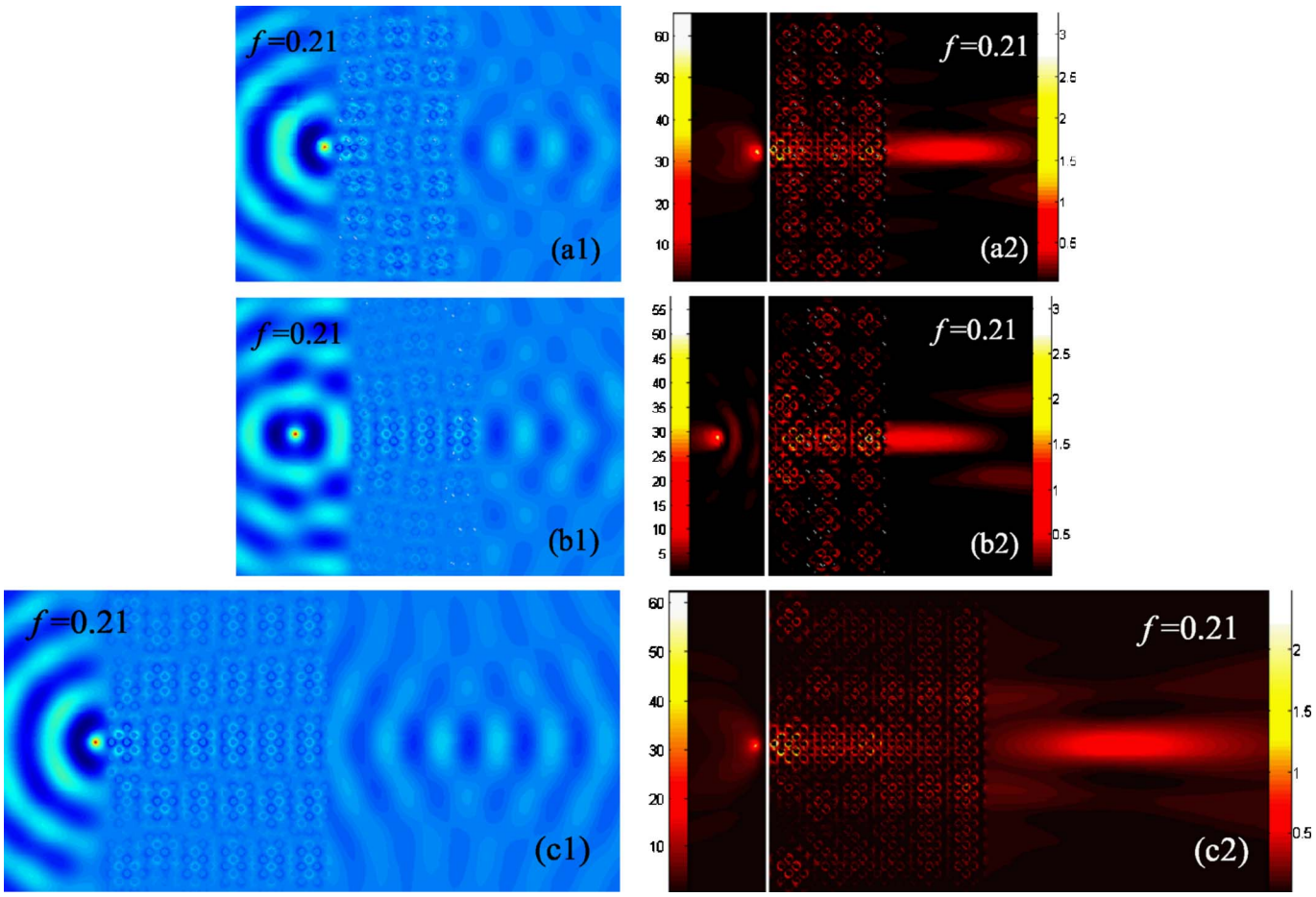

Fig. 8. (Color online) Imaging analysis for the PhC slabs at $f=0.21$. A point source is located at (a) $d_o=1.5a$ and (b) $d_o=6a$ before a 17-layer slab, (c) Point source located at $d_o=1.5a$ before a 29-layer slab. (a1), (b1), and (c1) are the snapshots of the electric field amplitude. (a2), (b2), and (c2) display the corresponding intensity distributions.

PhC. Three kinds of focusing have been summarized and demonstrated by numerical simulations. Although the theoretical analyses of Bloch waves are calculated for infinite PhCs, they are still well consistent with the numerical simulations. In this paper, our analysis has been focused on a dielectric cylindrical square-lattice PhC, but it also can be extended to others such as triangular-lattice cylindrical and elliptical-rod square-lattice PhCs.

ACKNOWLEDGMENTS

This work is partially supported by the Natural Science Foundation of China (grants 10576012 and 60538010), the National High Technology Research and Development Program of China (grant 2004AA84ts12), and the Specialized Research Fund for the Doctoral Program of Higher Education of China (grant 20040532005).

Z. Tang's e-mail address is tangzx1000@163.com.

REFERENCES

1. E. Yablonovitch, "Inhibited spontaneous emission in solid-state physics and electronics," Phys. Rev. B **58**, 2059–2062 (1987).
2. S. John, "Strong localization of photons in certain disordered dielectric superlattices," Phys. Rev. Lett. **58**, 2486–2489 (1987).
3. M. Notomi, "Theory of light propagation in strongly modulated photonic crystals: refractionlike behavior in the vicinity of the photonic band gap," Phys. Rev. B **62**, 10696–10705 (2000).
4. C. Luo, S. G. Johnson, J. D. Joannopoulos and J. B. Pendry, "All-negative refraction without negative effective index," Phys. Rev. B **65**, 201104(R) (2002).
5. V. G. Veselago, "The electrodynamics of substances with simultaneously negative values of ε and μ," Sov. Phys. Usp. **10**, 509–514 (1968).
6. J. B. Pendry, "Negative refraction makes a perfect lens," Phys. Rev. Lett. **85**, 3966–3969 (2000).
7. R. A. Shelby, D. R. Smith, and S. Schultz, "Experimental verification of a negative index of refraction," Science **292**, 77–79 (2001).
8. E. Cubukcu, K. Aydin, E. Ozbay, S. Foteinopoulou, and C. M. Soukoulis, "Negative refraction by photonic crystals," Nature **423**, 604–605 (2003).
9. P. V. Parimi, W. T. Lu, P. Vodo, and S. Sridhar, "Imaging by flat lens using negative refraction," Nature **426**, 404–404 (2003).
10. S. Foteinopoulou and C. M. Soukoulis, "Negative refraction and left-handed behavior in two-dimensional photonic crystals," Phys. Rev. B **67**, 235107 (2003).
11. R. Moussa, S. Foteinopoulou, L. Zhang, G. Tuttle, K. Guven, E. Ozbay, and C. M. Soukoulis, "Negative refraction and superlens behavior in a two-dimensional photonic crystal," Phys. Rev. B **71**, 085106 (2005).
12. X. Ao and S. He, "Negative refraction of left-handed

behavior in porous alumina with infiltrated silver at an optical wavelength," Appl. Phys. Lett. **87**, 101112 (2005).
13. R. Gajić, R. Meisels, F. Kuchar, and K. Hingerl, "Refraction and rightness in photonic crystals," Opt. Express **13**, 8596–8605 (2005).
14. Z. Tang, R. Peng, D. Fan, S. Wen, H. Zhang, and L. Qian, "Absolute left-handed behaviors in a triangular elliptical-rod photonic crystal," Opt. Express **13**, 9796–9803 (2005).
15. X. Zhang, "Image resolution depending on slab thickness and object distance in a two-dimensional photonic-crystal-based superlens," Phys. Rev. B **70**, 195110 (2004).
16. C.-H. Kuo and Z. Ye, "Flat lens imaging does not need negative refraction," arxiv.org:http://arxiv.org/abs/cond-mat/0312288.
17. C.-H. Kuo and Z. Ye, "Negative-refraction-like behavior revealed by arrays of dielectric cylinders," Phys. Rev. E **70**, 026608 (2004).
18. H.-T. Chien, H.-T. Tang, C.-H. Kuo, C.-C. Chen, and Z. Ye, "Direct diffraction without negative refraction," Phys. Rev. B **70**, 113101 (2004).
19. L.-S. Chen, C.-H. Kuo, and Z. Ye, "Guiding optical flows by photonic crystal slabs made of dielectric cylinders," Phys. Rev. E **69**, 066612 (2004).
20. S. Feng, Z.-Y. Li, Z.-F. Feng, B.-Y. Cheng, and D.-Z. Zhang, "Imaging properties of an elliptical-rod photonic-crystal slab lens," Phys. Rev. B **72**, 075101 (2005).
21. K. Ren, S. Feng, Z.-F. Feng, Y. Sheng, Z.-Y. Li, B.-Y. Cheng, and D.-Z. Zhang, "Imaging properties of triangular lattice photonic crystal at the lowest band," Phys. Rev. A **348**, 405–409 (2006).
22. K. Sakoda, *Optical Properties of Photonic Crystals* (Springer-Verlag, 2001).
23. L.-M. Li and Z.-Q. Zhang, "Multiple-scattering approach to finite-sized photonic band-gap materials," Phys. Rev. B **58**, 9587–9590 (1998).
24. H. Kosaka, A. Tomita, T. Kawashima, T. Sato, and S. Kawakami, "Splitting of triply degenerate refractive indices by photonic crystals," Phys. Rev. B **62**, 1477–1480 (2000).